

# Nematic topological semimetal and insulator in magic angle bilayer graphene at charge neutrality

Shang Liu, Eslam Khalaf, Jong Yeon Lee, and Ashvin Vishwanath

*Department of Physics, Harvard University, Cambridge, MA 02138*

(Dated: September 2, 2022)

We report on a fully self-consistent Hartree-Fock calculation of interaction effects on the Moiré flat bands of twisted bilayer graphene, assuming that valley  $U(1)$  symmetry is respected. We use realistic band structures and interactions and focus on the charge neutrality point, where experiments have variously reported either insulating or semimetallic behavior. Restricting the search to orders for which the valley  $U(1)$  symmetry remains unbroken, we find three types of self-consistent solutions with competitive ground state energy (i) insulators that break  $C_2\mathcal{T}$  symmetry, including valley Chern insulators (ii) spin or valley polarized insulators and (iii) rotation  $C_3$  symmetry breaking semimetals whose gaplessness is protected by the topology of the Moiré flat bands. We find that the relative stability of these states can be tuned by weak strains that break  $C_3$  rotation. The nematic semimetal and also, somewhat unexpectedly, the  $C_2\mathcal{T}$  breaking insulators, are stabilized by weak strain. These ground states may be related to the semi-metallic and insulating behaviors seen at charge neutrality, and the sample variability of their observation. We also compare with the results of STM measurements and quantum oscillations near charge neutrality.

**Introduction** — The discovery of interaction-driven insulating and superconducting behavior in twisted bilayer graphene (TBG) [1, 2] has inspired intensive efforts to understand this behavior [3–16] and to find related systems which exhibit similar phenomenology [17–22]. This work has started to bear fruit with several groups announcing similar observations in TBG samples [23–26] as well as other Moiré materials [27–31]. The basic mechanism underlying the enhancement of correlation in these materials is understood to originate from the long-wavelength Moiré pattern leading to quenching of the electron kinetic energy manifested in flat energy bands [32, 33]. Nevertheless, the nature of the observed correlated insulating states remains under debate [4–6, 8, 9].

Early experiments found clear signature of a correlated insulating state at half-filling [34] [1, 23]. Subsequently, insulating ferromagnetic states were also observed at quarter and three-quarter fillings [23, 24]. On the other hand, in all these experiments [1, 2, 23] insulating behavior was absent at charge neutrality (CN) where signatures of semimetallic behavior were observed instead. In contrast, a recent experiment surprisingly found an insulator at CN whose transport gap was larger than those at  $1/2$ ,  $1/4$  and  $3/4$  fillings [25].

On the theory side, it was realized early on [4, 35] that a simple Mott picture for the insulating phase is complicated by the band topology which prohibits the construction of localized orbitals describing the flat bands while preserving all the symmetries. Various orders have been proposed to account for the insulating states. At charge neutrality, a  $C_2\mathcal{T}$  symmetry breaking insulator, with Chern number  $\pm 1$  for each spin and valley flavour was proposed in [9], along with a  $C_2\mathcal{T}$  symmetry preserving insulator that is believed to require mixing with remote bands [9]. An intervalley coherent order [4] was proposed as a candidate for the insulating state at half-filling while nematic orders were discussed in [6, 11] and ferromagnetic ordering was proposed in [8]. In the presence of explicit  $C_2$  symmetry breaking induced by a substrate, valley or spin polarized insulator with valley resolved Chern numbers have been discussed [17, 36].

In this letter, we perform a self-consistent Hartree-Fock mean field analysis for the screened Coulomb interaction projected onto the flat bands.

We focus on the CN point because of its pivotal role in determining the entire phase diagram. We will discuss other fillings in subsequent work. For simplicity, we restrict our attention to orders that conserve the  $U(1)$  valley charge as well as translation invariance at the scale of the Moiré unit cell. Our results include the expected spin-polarized and valley-polarized insulators, which break no other symmetries. In addition we observe a strong tendency to breaking spatial rotation symmetries. We find a  $C_2\mathcal{T}$ -breaking insulator and two distinct  $C_2\mathcal{T}$ -symmetric semimetallic phases which break  $C_3$ -symmetry. The  $C_2\mathcal{T}$ -breaking phase has a Chern number of  $C = \pm 1$ , per flavor (i.e. valley and spin). Different spin/valley orderings then lead to various ground states ranging from quantum anomalous Hall (QAH) to quantum valley Hall (QVH) or quantum spin Hall (QSH) insulators with very similar Hartree-Fock energies. Of these, the QVH insulator breaks  $C_2$  symmetry, allowing for a direct coupling to the  $C_2$ -breaking hBN substrate, potentially favoring it in situations where the sample and substrate are aligned. The gapless  $C_3$ -breaking phases are obtained by bringing the two Dirac cones from the Moiré  $K$  and  $K'$  very close to the  $\Gamma$  point. Instead of merging and opening a gap as one might normally expect, the Dirac points remain gapless since they carry the same chirality [4], a consequence of descending from the Dirac points of graphene from the same valley for the two layers. This topological protection prevents them from annihilating, resulting in a gapless semimetallic state. Thus, the metallic nature at CN in this scenario is intimately tied to the topological properties of the magic angle flat bands.

We investigate the effect of small explicit  $C_3$  symmetry breaking which can arise in real samples due to strain [21], and show that it strongly influences the competition between different symmetry broken phases, favoring one of the  $C_3$ -breaking semimetallic phases. Surprisingly, the  $C_2\mathcal{T}$ -breaking insulators also exhibits a strong susceptibility to  $C_3$

symmetry breaking. The energies of the insulating  $C_2\mathcal{T}$ -breaking and the semimetallic  $C_2\mathcal{T}$ -preserving states are lowered compared to the spin/valley ferromagnets, and approach each other quickly as the value of the  $C_3$ -breaking parameter is increased. Our results suggest that these two states are candidate ground states in the presence of very small explicit  $C_3$  symmetry breaking which is likely to exist in experiments. Further competition between these two phases is likely to be settled by small sample-dependent details, potentially explained by the realization of an insulator in some samples and a semimetal in other samples.

**Problem setup** — The single-particle physics is described by the Bistritzer-MacDonald (BM) model [32, 33], which employs a continuum approximation close to  $K$  and  $K'$  for a pair of graphene sheets rotated relative to each other by an angle  $\theta$ . The Hamiltonian for the  $K$  valley is given by:

$$\mathcal{H}_+ = \sum_l \sum_{\mathbf{k}} f_l^\dagger(\mathbf{k}) h_{\mathbf{k}}(l\theta/2) f_l(\mathbf{k}) + \left( \sum_{\mathbf{k}} \sum_{i=1}^3 f_t^\dagger(\mathbf{k} + \mathbf{q}_i) T_i f_b(\mathbf{k}) + h.c. \right). \quad (1)$$

Here,  $l = t/b \simeq \pm 1$  is the layer index, and  $f_l(\mathbf{k})$  is the  $K$ -valley electron originated from layer  $l$ .  $h_{\mathbf{k}}(\theta)$  is the monolayer graphene  $K$ -valley Hamiltonian with twist angle  $\theta$  (see supplemental material for details) and  $\mathbf{q}_1$  is defined as  $K_b - K_t$  with  $K_l$  denoting the  $K$ -vector of layer  $l$ .  $\mathbf{q}_2 = O_3 \mathbf{q}_1$  is the counterclockwise  $2\pi/3$  rotation of  $\mathbf{q}_1$ , and  $\mathbf{q}_3 = O_3 \mathbf{q}_2$ . Finally, the interlayer coupling matrices are given by

$$T_j = \begin{pmatrix} w_0 & w_1 e^{-(j-1)\frac{2\pi i}{3}} \\ w_1 e^{(j-1)\frac{2\pi i}{3}} & w_0 \end{pmatrix}, \quad (2)$$

with  $w_0$  and  $w_1$  denoting intrasublattice and intersublattice hopping, respectively. Due to lattice relaxation effects, which shrink the AA regions relative to the AB regions, the value of  $w_0$  at the magic angle is about 75% of  $w_1$  [37, 38]. Throughout this work, we will use the values  $w_1 = 110$  meV and  $w_0 = 82.5$  meV. Explicit  $C_3$  symmetry breaking is implemented via the substitution  $T_1 \rightarrow (1 + \beta)T_1$  [39].

To study possible correlated insulating states, we employ a momentum-space self-consistent Hartree-Fock mean field theory. The momentum-space description allows us to focus on the pair of flat bands at CN, thereby evading the difficulties associated with the real space Wannier obstruction rooted in the fragile topology of these bands [4, 35, 40]. Restricting the analysis to the flat bands is only justified in the limit when both the bandwidth and interaction strength are much smaller than the bandgap. For realistic interactions, the interaction strength is of the same order as the bandgap which means that symmetry-broken states involving remote bands cannot be ruled out [9]. Given the strong angle dependence and appearance of correlated states only near the magic angle [1, 2, 23], it is likely that the relevant symmetry-broken phases experimentally originate mostly from the two flat bands which

justifies our approximation.

The Hartree-Fock (HF) mean field theory is defined in terms of the projector

$$P_{\alpha,\beta}(\mathbf{k}) = \langle c_\alpha^\dagger(\mathbf{k}) c_\beta(\mathbf{k}) \rangle, \quad P(\mathbf{k})^2 = P(\mathbf{k}) = P(\mathbf{k})^\dagger, \quad (3)$$

where  $c_\alpha(\mathbf{k})$  is the annihilation operator for an electron at momentum  $\mathbf{k}$  and  $\alpha = (n, \tau, s)$  is a combined index for band, valley and spin, respectively. For a gapped or semimetallic phase at CN,  $P$  satisfies  $\text{tr } P(\mathbf{k}) = 4$  [41]. depend for all  $\mathbf{k}$  points The HF mean field Hamiltonian has the form

$$\mathcal{H}_{\text{MF}} = \sum_{\mathbf{k}} \{ c(\mathbf{k})^\dagger [h_0(\mathbf{k}) + h_{\text{HF}}(P, \mathbf{k})] c(\mathbf{k}) - \frac{1}{2} \text{tr } h_{\text{HF}}(P, \mathbf{k}) P^T(\mathbf{k}) \}. \quad (4)$$

Here,  $c(\mathbf{k})$  is a column vector in the index  $\alpha$ ,  $h_0(\mathbf{k})$  denotes the single particle Hamiltonian and  $h_{\text{HF}}(\mathbf{k})$  is given by

$$h_{\text{HF}}(P, \mathbf{k}) = \frac{1}{A} \sum_{\mathbf{G}} V_{\mathbf{G}} \Lambda_{\mathbf{G}}(\mathbf{k}, \mathbf{k}) \sum_{\mathbf{k}'} \text{tr } P^T(\mathbf{k}') \Lambda_{\mathbf{G}}^\dagger(\mathbf{k}', \mathbf{k}') - \frac{1}{A} \sum_{\mathbf{G}, \mathbf{k}'} V_{\mathbf{G}+\mathbf{k}'-\mathbf{k}} \Lambda_{\mathbf{G}}(\mathbf{k}, \mathbf{k}') P^T(\mathbf{k}') \Lambda_{\mathbf{G}}^\dagger(\mathbf{k}, \mathbf{k}'), \quad (5)$$

where  $A$  is the total area. The  $\mathbf{k}'$  summation ranges over the first Brillouin zone whereas the  $\mathbf{G}$  summation is over reciprocal lattice vectors.  $V(\mathbf{q})$  is the interaction potential which we take to be a single-gate-screened Coulomb interaction  $V(\mathbf{q}) = \frac{e^2}{2\epsilon\epsilon_0 q} (1 - e^{-2qd_s})$  with dielectric constant  $\epsilon = 7$  and screening length equal to the gate distance  $d_s \approx 40$  nm.

The first term in (5) is the Hartree term while the second is the Fock term. The matrix  $\Lambda_{\mathbf{G}}(\mathbf{k}, \mathbf{k}')$  contains the form factors for the single-particle wavefunctions satisfying  $u_{n,\tau;\mathbf{G}}(\mathbf{k} + \mathbf{G}_0) = u_{n,\tau;\mathbf{G}+\mathbf{G}_0}(\mathbf{k})$ . It is given by

$$[\Lambda_{\mathbf{G}}(\mathbf{k}, \mathbf{k}')]_{\alpha,\alpha'} = \delta_{s,s'} \delta_{\tau,\tau'} \langle u_{n,\tau}(\mathbf{k}) | u_{n',\tau}(\mathbf{k}' + \mathbf{G}) \rangle. \quad (6)$$

The HF self-consistent analysis starts by proposing an ansatz for the projector  $P(\mathbf{k})$ , then substituting in the Hamiltonian (4) which is then used to compute the new projector. This procedure is iterated until convergence is achieved.

One important subtlety in the HF approach is that the band structure depends on the filling even without symmetry breaking. This follows from the fact that the form factor matrix  $\Lambda_{\mathbf{q}}(\mathbf{k})$  is not diagonal in the band index for  $\mathbf{q} \neq 0$  since  $u$ -vectors from different bands are not orthogonal at different momenta. In addition, the Hartree term contains a trace over all filled bands which also affects the dispersion of the empty bands. This means that the band structure obtained from the BM model is only valid at a specific filling which determines the references point for our analysis. At this point, it will be assumed that interaction effects are already included in the parameters of the effective model which can be obtained by fitting to *ab initio* calculations or comparing to STM data away from the magic angles [42]. A natural choice of the reference

point, which we adopt throughout this letter, is the CN point. This means that the single particle Hamiltonian  $h_0(\mathbf{k})$  is given by

$$h_0(\mathbf{k}) = h_{\text{BM}}(\mathbf{k}) - h_{\text{HF}}(P_0, \mathbf{k}) \quad (7)$$

where  $h_{\text{BM}}(\mathbf{k})$  is the BM Hamiltonian and  $P_0$  is the projector corresponding to symmetry unbroken state obtained by filling the lower band of the BM Hamiltonian at CN. We note that in the different approach of Ref. [9] where multiple bands are included, the reference point was taken in the limit of decoupled layers. In our complementary approach of projection onto the flat bands it is not possible to implement such a choice.

Using CN as our reference point implies that the bands at empty or full filling should include some HF corrections leading to a modified band structure. The resulting DOS is shown in Fig. 3a. We notice that the separation between the two peaks in the DOS is about 10-15 meV in agreement with the measured DOS in STM experiments [42]. Thus, our approach provides an explanation for the discrepancy between the experimentally measured peak separation and the expectation based on the BM model whose bandwidth close to the magic angle is much smaller (1-3 meV).

**Symmetry-broken phases.** — The interacting TBG Hamiltonian is characterized by the following symmetries [4]: spinless time-reversal  $\mathcal{T}$ ,  $\text{SU}(2)$  spin rotation,  $\text{U}(1)$  valley charge conservation and  $C_6$  symmetry as well as a mirror symmetry which switches layers and sublattices but acts within each valley. Of these, only spin rotation,  $C_3$ , mirror and  $C_2\mathcal{T}$  act within each valley. At integer filling, different correlated insulating phases can emerge by breaking some of these symmetries. Time-reversal symmetry is broken by valley polarized (VP) states, where the filling of the two valleys is different. Spin rotation symmetry is broken by spin polarization (SP) leading to ferromagnetic order.  $\text{U}(1)$  valley charge conservation is broken in the presence of intervalley coherent (IVC) superposition of states from the two valleys.  $C_2$  symmetry is broken by sublattice polarization which gaps out the Dirac points at the Moiré  $K$  and  $K'$  points.

Breaking  $C_3$  symmetry alone does not generally lead to a gapped phase since it only moves the Dirac points away from the Moiré  $K$  and  $K'$  without gapping them out. Even strong  $C_3$  breaking does not result in the merging and gapping of the Dirac nodes, in contrast with other familiar band structures such as single layer graphene. This follows from the fact that the chirality of the Dirac nodes, which is well defined in the presence of  $C_2\mathcal{T}$  symmetry, is the equal [4, 15], rather than opposite. Alternately, one can phrase the argument as follows. The topology of the two flat bands is captured by the second Stiefel-Whitney invariant  $w_2$  [40, 43, 44]. This invariant is protected by  $C_2\mathcal{T}$  and only depends on the flat band eigenstates which are unaffected by any symmetry breaking that does not involve other bands (which is the main assumption in this work). Indeed, the  $w_2$  invariant must be trivial for a single isolated band, implying we cannot separate the pair of connected flat bands [45]. Thus the non-trivial  $w_2$  invariant

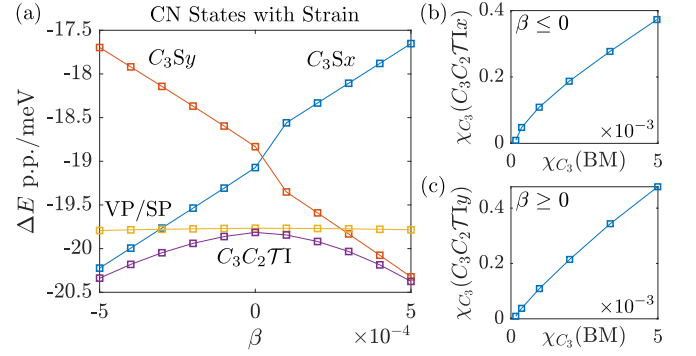


FIG. 1. (a) Energies of the solutions of the self-consistent HF equations as a function of the  $C_3$  symmetry breaking parameter  $\beta$ . All energies are measured relative to the state with no-broken symmetry. The degree of  $C_3$ -breaking measured by  $\chi_{C_3}$  (Eq. 8) for the  $C_2\mathcal{T}$ -breaking insulator as a function  $\chi_{C_3}$  for the non-interacting system for  $0 \leq |\beta| \leq 5 \times 10^{-4}$  are shown in panels (b) and (c) for positive and negative values of  $\beta$ , respectively.

implies that the two Dirac points cannot be removed without breaking  $C_2\mathcal{T}$ .

Before presenting the numerical results, let us make the following observations. First, it is relatively easy to show that a state with uniform full spin or valley polarization is always a self-consistent solution to the HF equations at CN for sufficiently narrow bands. These two states have the same energy in the absence of Hund's coupling [17, 22]. The IVC state is known to have higher energy than SP/VP states for isolated bands with non-vanishing valley Chern number [17, 36]. These arguments do not generalize to TBG where the extra  $C_2$  symmetry complicates the discussion (see supplemental material and Ref. [46]). Nevertheless, we will exclude IVC orders from our numerical analysis (which is equivalent to assuming unbroken  $\text{U}(1)$  valley charge conservation) since it leads to significant simplification by allowing us to focus on a single flavor (spin and valley). Different diagonal spin-valley orders can then be generated from the single-flavor solution by applying different symmetries. The energy competition with  $\text{U}(1)$  valley symmetry broken phases is considered in [46].

**Results** — The results for the self-consistent HF analysis are provided in Fig. 1 showing the energies of the different solutions as a function of the  $C_3$  symmetry breaking parameter  $\beta$ . There are two types of gapped solutions corresponding to either flavor-polarized (spin/valley) states or  $C_2\mathcal{T}$ -breaking ( $C_2\mathcal{T}I$ ) insulators. There are three gapped solutions corresponding to spin-polarized (SP), valley-polarized (VP) and  $C_2\mathcal{T}$ -breaking ( $C_2\mathcal{T}I$ ) insulators. The latter does not break  $C_3$  when  $\beta = 0$  but develops a large  $C_3$  breaking component for  $\beta \neq 0$ . The extent of  $C_3$  symmetry breaking can be quantified by defining

$$\chi_{C_3} = \frac{1}{N} \sum_{\mathbf{k}} (1 - |\langle \psi_{O_3\mathbf{k}} | C_3 | \psi_{\mathbf{k}} \rangle|^2), \quad (8)$$

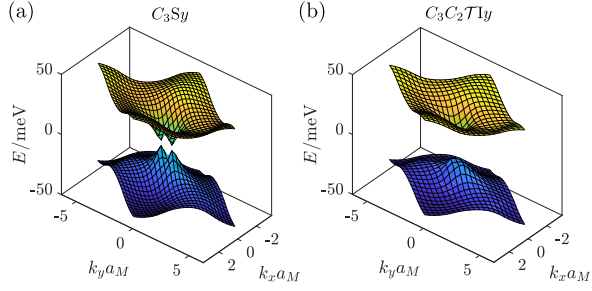


FIG. 2. 3D band structure for one of the (a)  $C_3$ -breaking semimetals and (b)  $C_2\mathcal{T}$  breaking valley Hall insulators.

which vanishes for any  $C_3$ -symmetric state. Here,  $|\psi_{\mathbf{k}}\rangle$  are the occupied single-particle eigenstates of the HF Hamiltonian with momentum  $\mathbf{k}$  (for a given flavor). The value of  $\chi_{C_3}$  for the  $C_2\mathcal{T}$  state is shown in Fig. 1 as a function of  $\chi_{C_3}$  for the corresponding non-interacting states arising from explicit  $C_3$ -breaking parameter  $\beta \neq 0$  in the BM model. We can clearly see from the figure that a relatively small  $\chi_{C_3}(BM) \sim 10^{-3}$  in the non-interacting states induces a much larger  $C_3$  symmetry breaking of almost two orders of magnitude in the  $C_2\mathcal{T}$  state. This serves to show that the  $C_2\mathcal{T}$  has very large susceptibility to  $C_3$  symmetry breaking. In the following, we will refer to this state for positive and negative  $\beta$  as  $C_3C_2\mathcal{T}1y$  and  $C_3C_2\mathcal{T}1x$ , respectively. In addition to this insulating state, there are two distinct  $C_2$ -preserving semimetallic phases which spontaneously break  $C_3$  even for  $\beta = 0$  which we denote by  $C_3Sx$  and  $C_3Sy$ , since they have Dirac points along  $k_x$  and  $k_y$ , respectively. We notice that these ground states are similar to the ones obtained within a 10-band model Ref. [42] which used a site-local ansatz for the interactions.

The  $C_2\mathcal{T}$  phase obtained here is characterized by a Chern number of  $\pm 1$  for a given spin and valley. The nature of the resulting phase depends on the precise symmetries which are broken as follows: (i) if  $\mathcal{T}$  is broken but  $C_2$  and spin rotation are preserved, we obtain a quantum anomalous Hall (QAH) insulator with total Chern number  $C = \pm 4$ , (ii) if spin rotation is broken we obtain a quantum-spin Hall (QSH) insulator with opposite Chern number  $C_s = \pm 2$  for opposite spins, (iii) if  $C_2$  is broken but  $\mathcal{T}$  and spin rotation symmetry are preserved, then a quantum valley Hall (QVH) insulator obtains with opposite Chern number  $C_v = \pm 2$  for opposite valleys, or (iv) we can additionally break spin rotation symmetry to obtain a state where opposite spins within the same valley also have opposite Chern numbers resulting in a quantum spin-valley Hall (QSVH) insulator where flipping either spin or valley flips the Chern number. The QH, QSH and QVSH preserve either  $C_2$  or a combination of  $C_2$  and some internal symmetries, thus the only state expected to couple to the  $C_2$ -breaking hBN substrate is the QVH which is likely to be energetically favored in aligned samples[47]. The energies of the four possible  $C_2\mathcal{T}$  states are very similar differing only by very small  $\sim 10^{-3}$  meV Hartree corrections. Similarly, the flavor-polarized state can be spin-polarized, breaking  $SU(2)$

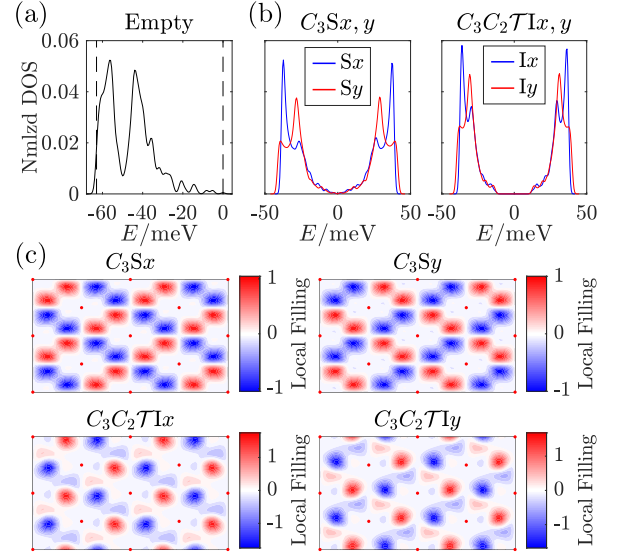


FIG. 3. (a) Normalized DOS of the empty filling band structure. The two vertical dashed lines indicate the band bottom and top which is chosen to be at  $E = 0$ . (b) Normalized DOS and (c) local filling fraction for the upper layer defined in (9) for the four potential ground states for strain parameter  $\beta = \pm 4 \times 10^{-4}$ . For positive (negative) beta: the two competing ground states are a  $C_2\mathcal{T}$ -preserving semimetal  $C_3Sy$  ( $C_3Sx$ ) and a  $C_2\mathcal{T}$ -breaking valley Hall insulator  $C_3C_2\mathcal{T}1y$  ( $C_3C_2\mathcal{T}1x$ ), both strongly breaking  $C_3$ . The red dots in (c) indicates the AA position. In (c) the breaking of  $C_2$  and  $C_3$  rotation symmetries are clearly visible.

spin rotation, valley-polarized breaking  $\mathcal{T}$  or a spin-valley-locked states which breaks both but preserves a combination of  $\mathcal{T}$  and  $\pi$ -spin rotation. These states are degenerate on the mean field level and are only distinguished by intervalley Hund's coupling [17, 22] neglected in this study.

At  $\beta = 0$ , the energies of the insulating VP/SP and  $C_2\mathcal{T}$  states are very close and smaller by about 1 meV per particle than the energies of the two semimetallic  $C_3$  breaking states. An explanation for this fact is detailed in the supplemental material in the chiral limit where the intrasublattice hopping is switched off [48]. In this limit, we can establish rigorous bounds for the energy of the different phases and show that the lowest energy states are the SP/VP and the  $C_2\mathcal{T}$  state whose energy is higher by a very small amount. The energies of the  $C_3S$  states are higher than these two but the energy difference can be shown to be relatively small (compared to the interaction scale) provided that the form factors (Eq. 6) decay quickly enough in  $|\mathbf{G}|$  and  $|\mathbf{k} - \mathbf{k}'|$ , which can be confirmed numerically. This analysis explains why these states are expected to be close in energy, but it is generally insufficient to capture the details of the energy competition which depends sensitively on the intrasublattice hopping  $w_0$  and can only be determined numerically.

Once  $\beta$  becomes non-zero, the energy of the  $C_2\mathcal{T}$  breaking state is reduced relative to the VP/SP state. Furthermore, one of the two  $C_3$ -breaking states (depending on the sign of  $\beta$ ) goes down in energy becoming more energetically favorable

to the VP/SP state around  $\beta = \pm 3 \times 10^{-4}$ . For larger values of  $\beta \gtrsim 4 \times 10^{-4}$ , the energies of the insulating  $C_2\mathcal{T}$ -breaking phase and the semimetallic  $C_2\mathcal{T}$ -preserving phase approach the same value. This indicates that even very small explicit  $C_3$ -breaking picks out these two states as the main candidates for the ground state at CN. Assuming that such small explicit  $C_3$  symmetry breaking exists in real samples due to strain, our analysis leads to the conclusion that the ground state of TBG at CN is either a  $C_2\mathcal{T}$ -breaking insulator or a  $C_2\mathcal{T}$ -symmetric semimetal. Both states strongly break  $C_3$  symmetry and are very close in energy. It is worth noting that, in the presence of disorder, massless Dirac fermions may also emerge from the spatial domain walls of locally  $C_2\mathcal{T}$  breaking insulating regions [49].

**Consequences for Experiment** The possibility of  $C_3$  breaking at CN is consistent with several recent reports [42, 50, 51] which observed direct evidence of  $C_3$  breaking in STM measurements. To check the compatibility of these measurements with our mean-field solutions, we compute the DOS for the four possible  $C_3$ -breaking states (arising for positive or negative values of  $\beta$ ) in Fig. 3b. We see that in all cases the global DOS consists of two broad peaks (which are sometimes further split into two) separated by about 60-80 meV, in agreement with the STM measurements [42, 50]. The DOS alone however, is insufficient to distinguish the insulating and semi-metallic state, since both have very low DOS close to zero energy. One way to distinguish the two is to compute the local filling fraction defined as [51]

$$\nu(\mathbf{r}) = 8 \left( \frac{\rho_{\text{LB}}(\mathbf{r})}{\rho_{\text{LB}}(\mathbf{r}) + \rho_{\text{UB}}(\mathbf{r})} - \frac{1}{2} \right) \in [-4, 4], \quad (9)$$

where  $\rho_{\text{LB/UB}}(\mathbf{r})$  denote the integrated local DOS from the upper layer for the lower/upper band.  $\nu(\mathbf{r})$ , shown in Fig. 3, exhibits clear  $C_3$ -symmetry breaking pattern for all the four phases. The patterns for the  $C_3\text{S}$  and  $C_3C_2\mathcal{T}\text{I}$  QVH phases can be distinguished by  $C_2$  symmetry which is visibly present in the former but absent in the latter (the pattern of the other  $C_3C_2\mathcal{T}\text{I}$  is obtained by symmetrizing the QVH result relative to  $C_2$  with the result being very similar to the one for the  $C_3\text{S}$  breaking states up to an overall factor). The  $C_3\text{S}$  pattern is qualitatively similar to that measured in Ref. [51], with the density vanishing at the Kagomé lattice site lying on the mirror plane and changing sign twice around it, while having non-vanishing magnitude with opposite signs on the other two Kagomé lattice sites. Such structure is generic for any  $C_3$ -breaking phase which preserves mirror and particle-hole symmetries [52] and a combination of  $C_2$  and some local symmetry. [53]

Another compatibility check is to compare the expected sequence of Landau levels generated by our mean field solutions to the experimentally measured ones. In this regard, we note that a pattern of  $C_3$  symmetry breaking was recently proposed [39] as an explanation for the unusual sequence of Landau levels ( $n_e/n_B = \pm 4, \pm 8, \pm 12, \dots$ ) observed for the semimetallic state at CN [1, 23]. Naively, the two Moiré

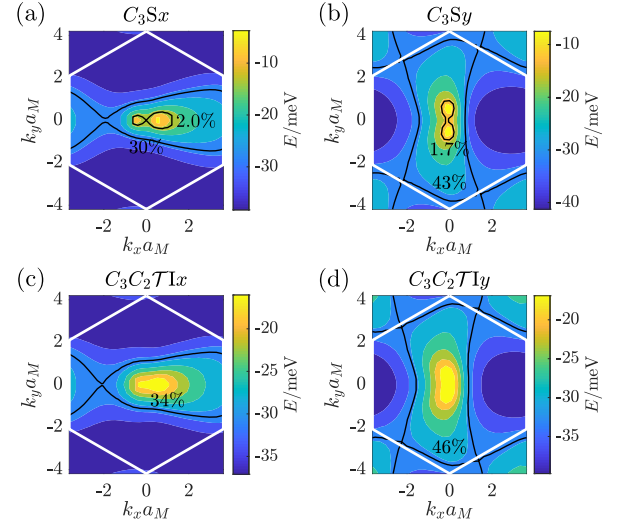


FIG. 4. Hole-doping Fermi surfaces in the plus valley for the (a)  $C_3\text{S}x$  state (b)  $C_3\text{S}y$ , (c)  $C_3C_2\mathcal{T}\text{I}x$ , and (d)  $C_3C_2\mathcal{T}\text{I}y$  states. The contours corresponding to the van Hove singularities are highlighted.

Dirac cones, each of which is four-fold degenerate due to spin and valley degrees of freedom, give rise to a Landau level degeneracy of eight. However, in the presence of  $C_3$  breaking, the two Dirac points are pushed towards each other so that the two electron pockets at small doping merge into one at the doping is increased. The Fermi surface contours for the lower band in the two  $C_3$  breaking semimetals are provided in Fig. 4 showing the two electron pockets corresponding to the two nearby Dirac points quickly merging into a single one for doping around 0.02 (per spin per valley). This doping corresponds to a magnetic field of  $\sim 0.5$  T in agreement with experimental observations. This mechanism was previously pointed out in Ref. [39]. We note that this conclusion holds regardless of the nature of  $C_3$  symmetry breaking, in contrast to the case of weak  $C_3$  breaking that requires a particular sense of the breaking [39].

Finally, we propose one additional experimental check for the  $C_2\mathcal{T}$ -breaking insulating state by investigating the response of the gap to in-plane magnetic field. Since spin symmetry is unbroken, we expect the gap to close with a slope of approximately  $2\mu_B$  due to Zeeman splitting. We note that, as pointed out recently in the context of twisted double bilayer graphene [22], in-plane field can also induce an orbital effect. For the state considered here, this effect turned out to be rather small (see supplemental material) and it only slightly changes the slope of the gap reduction with in-plane field. It is worth mentioning that, although this feature is not unique to the  $C_2\mathcal{T}$ -breaking insulator discussed here, it can be used to exclude competing states such as the spin-polarized insulator.

**Conclusion** — In conclusion, we have performed a momentum-space self-consistent Hartree-Fock analysis to uncover the nature of the symmetry-broken phase in twisted bilayer graphene at charge neutrality. In addition to insulating states corresponding to spin, valley or sublattice polarization,



we found two  $C_3$ -breaking  $C_2\mathcal{T}$ -symmetric semimetallic solutions. Our main finding is that the existence of very small explicit  $C_3$ -breaking energetically favors one of these  $C_2\mathcal{T}$ -symmetric metallic state together with  $C_2\mathcal{T}$ -breaking insulating states. Both sets of states have similar energy within HF, strongly break  $C_3$  symmetry and are consistent with the density of states measured in STM experiments. They can be experimentally distinguished in transport measurements or by comparing space-resolved local filling fractions in STM. We propose these two states as candidates for the insulating and conducting states observed in different experiments at the CNP and suggest that the competition between the two is settled by small details that are likely sample-dependent.

*Acknowledgement.* — We thank Eva Andrei, Allan MacDonald, Adrian Po, A. Thomson and M. Xie for helpful discussions. S. L. A. V., J.Y. L. and E. K. were supported by a Simons Investigator Fellowship and by NSF-DMR 1411343. E. K. was supported by the German National Academy of Sciences Leopoldina through grant LPDS 2018-02 Leopoldina fellowship.

*Note added*— Following the completion of this work, a hidden symmetry in magic angle graphene was identified in [46] which weakens a lower bound established on the energy of IVCs, as discussed in the supplementary material. On extending the ground state search to include U(1) valley breaking orders [46], an intervalley coherent state that breaks the valley U(1) was found to be the ground state. However, assuming conservation of valley charge as done here, the lowest energy states are indeed the mean field solutions discussed above.

- 
- [1] Y. Cao, V. Fatemi, A. Demir, S. Fang, S. L. Tomarken, J. Y. Luo, J. D. Sanchez-Yamagishi, K. Watanabe, T. Taniguchi, E. Kaxiras, *et al.*, *Nature* **556**, 80 (2018).
  - [2] Y. Cao, V. Fatemi, S. Fang, K. Watanabe, T. Taniguchi, E. Kaxiras, and P. Jarillo-Herrero, *Nature* **556**, 43 (2018).
  - [3] C. Xu and L. Balents, *Phys. Rev. Lett.* **121**, 087001 (2018).
  - [4] H. C. Po, L. Zou, A. Vishwanath, and T. Senthil, *Phys. Rev. X* **8**, 031089 (2018).
  - [5] H. Isobe, N. F. Q. Yuan, and L. Fu, *Phys. Rev. X* **8**, 041041 (2018).
  - [6] A. Thomson, S. Chatterjee, S. Sachdev, and M. S. Scheurer, *Phys. Rev. B* **98**, 075109 (2018).
  - [7] Y.-Z. You and A. Vishwanath, arXiv preprint arXiv:1805.06867 (2018).
  - [8] J. Kang and O. Vafek, *Phys. Rev. X* **8**, 031088 (2018).
  - [9] M. Xie and A. H. MacDonald, arXiv preprint arXiv:1812.04213 (2018).
  - [10] Y.-P. Lin and R. M. Nandkishore, arXiv preprint arXiv:1901.00500 (2019).
  - [11] J. F. Dodaro, S. A. Kivelson, Y. Schattner, X. Q. Sun, and C. Wang, *Phys. Rev. B* **98**, 075154 (2018).
  - [12] B. Padhi, C. Setty, and P. W. Phillips, *Nano letters* **18**, 6175 (2018).
  - [13] F. Wu, A. H. MacDonald, and I. Martin, *Phys. Rev. Lett.* **121**, 257001 (2018).
  - [14] B. Lian, Z. Wang, and B. A. Bernevig, arXiv preprint arXiv:1807.04382 (2018).
  - [15] L. Zou, H. C. Po, A. Vishwanath, and T. Senthil, *Phys. Rev. B* **98**, 085435 (2018).
  - [16] B. Roy and V. Juričić, *Phys. Rev. B* **99**, 121407 (2019).
  - [17] Y.-H. Zhang, D. Mao, Y. Cao, P. Jarillo-Herrero, and T. Senthil, *Phys. Rev. B* **99**, 075127 (2019).
  - [18] E. Khalaf, A. J. Kruchkov, G. Tarnopolsky, and A. Vishwanath, *Phys. Rev. B* **100**, 085109 (2019).
  - [19] C. Mora, N. Regnault, and B. A. Bernevig, arXiv preprint arXiv:1901.05469 (2019).
  - [20] T. Cea, N. R. Walet, and F. Guinea, arXiv preprint arXiv:1903.08403 (2019).
  - [21] Z. Bi, N. F. Yuan, and L. Fu, arXiv preprint arXiv:1902.10146 (2019).
  - [22] J. Y. Lee, E. Khalaf, S. Liu, X. Liu, Z. Hao, P. Kim, and A. Vishwanath, arXiv preprint arXiv:1903.08685 (2019).
  - [23] M. Yankowitz, S. Chen, H. Polshyn, Y. Zhang, K. Watanabe, T. Taniguchi, D. Graf, A. F. Young, and C. R. Dean, *Science*, eaav1910 (2019).
  - [24] A. L. Sharpe, E. J. Fox, A. W. Barnard, J. Finney, K. Watanabe, T. Taniguchi, M. A. Kastner, and D. Goldhaber-Gordon, arXiv e-prints, arXiv:1901.03520 (2019).
  - [25] X. Lu, P. Stepanov, W. Yang, M. Xie, M. A. Aamir, I. Das, C. Urgell, K. Watanabe, T. Taniguchi, G. Zhang, A. Bachtold, A. H. MacDonald, and D. K. Efetov, arXiv preprint arXiv:1903.06513 (2019).
  - [26] E. Codecido, Q. Wang, R. Koester, S. Che, H. Tian, R. Lv, S. Tran, K. Watanabe, T. Taniguchi, F. Zhang, *et al.*, arXiv preprint arXiv:1902.05151 (2019).
  - [27] G. Chen, A. L. Sharpe, P. Gallagher, I. T. Rosen, E. Fox, L. Jiang, B. Lyu, H. Li, K. Watanabe, T. Taniguchi, *et al.*, arXiv preprint arXiv:1901.04621 (2019).
  - [28] G. Chen, L. Jiang, S. Wu, B. Lyu, H. Li, B. L. Chittari, K. Watanabe, T. Taniguchi, Z. Shi, J. Jung, *et al.*, *Nature Physics*, 1 (2019).
  - [29] X. Liu, Z. Hao, E. Khalaf, J. Y. Lee, K. Watanabe, T. Taniguchi, A. Vishwanath, and P. Kim, arXiv:1903.08130 (2019).
  - [30] C. Shen, N. Li, S. Wang, Y. Zhao, J. Tang, J. Liu, J. Tian, Y. Chu, K. Watanabe, T. Taniguchi, R. Yang, Z. Y. Meng, D. Shi, and G. Zhang, arXiv e-prints, arXiv:1903.06952 (2019).
  - [31] Y. Cao, D. Rodan-Legrain, O. Rubies-Bigordà, J. M. Park, K. Watanabe, T. Taniguchi, and P. Jarillo-Herrero, arXiv e-prints, arXiv:1903.08596 (2019).
  - [32] R. Bistritzer and A. H. MacDonald, *Proceedings of the National Academy of Sciences* **108**, 12233 (2011).
  - [33] J. M. B. Lopes dos Santos, N. M. R. Peres, and A. H. Castro Neto, *Phys. Rev. B* **86**, 155449 (2012).
  - [34] We follow the standard convention of measuring the filling relative to charge neutrality where the Dirac points of the original graphene sheet reside. Complete filling corresponds to  $\nu_T = 4$  while completely empty  $\nu_T = -4$  electrons per Moiré unit cell, accounting for both spin and valley degeneracy. Half filling corresponds to  $\nu_T = \pm 2$ .
  - [35] H. C. Po, L. Zou, T. Senthil, and A. Vishwanath, arXiv preprint arXiv:1808.02482 (2018).
  - [36] N. Bultinck, S. Chatterjee, and M. P. Zaletel, arXiv preprint arXiv:1901.08110 (2019).
  - [37] N. N. T. Nam and M. Koshino, *Phys. Rev. B* **96**, 075311 (2017).
  - [38] M. Koshino, N. F. Q. Yuan, T. Koretsune, M. Ochi, K. Kuroki, and L. Fu, *Phys. Rev. X* **8**, 031087 (2018).
  - [39] Y.-H. Zhang, H. C. Po, and T. Senthil, arXiv preprint arXiv:1904.10452 (2019).

- [40] H. C. Po, H. Watanabe, and A. Vishwanath, Phys. Rev. Lett. **121**, 126402 (2018).
- [41] For semimetals, this is true everywhere except for the gapless points where the projector is not defined.
- [42] Y. Choi, J. Kemmer, Y. Peng, A. Thomson, H. Arora, R. Polski, Y. Zhang, H. Ren, J. Alicea, G. Refael, F. von Oppen, K. Watanabe, T. Taniguchi, and S. Nadj-Perge, arXiv e-prints, arXiv:1901.02997 (2019).
- [43] J. Ahn, S. Park, and B.-J. Yang, Phys. Rev. X **9**, 021013 (2019).
- [44] B. Lian, F. Xie, and B. A. Bernevig, arXiv preprint arXiv:1811.11786 (2018).
- [45] In general, the total second Stiefel-Whitney number of two isolated bands is not equal to the sum of the second Stiefel-Whitney numbers separately for the two bands; there is an additional contribution from the first Stiefel-Whitney classes. In the special case we considered here, the  $C_3$  symmetry of the two-band subspace guarantees this additional term vanishes.
- [46] N. Bultinck, E. Khalaf, S. Liu, S. Chatterjee, A. Vishwanath, and M. P. Zaletel, arXiv preprint arXiv:1911.xxxxx (2019).
- [47] We thank A. Thomson for correspondence on this point.
- [48] G. Tarnopolsky, A. J. Kruchkov, and A. Vishwanath, Phys. Rev. Lett. **122**, 106405 (2019).
- [49] A. Thomson and J. Alicea, arXiv preprint arXiv:1910.11348 (2019).
- [50] A. Kerelsky, L. McGilly, D. M. Kennes, L. Xian, M. Yankowitz, S. Chen, K. Watanabe, T. Taniguchi, J. Hone, C. Dean, *et al.*, arXiv preprint arXiv:1812.08776 (2018).
- [51] Y. Jiang, J. Mao, X. Lai, K. Watanabe, T. Taniguchi, K. Haule, and E. Y. Andrei, arXiv preprint arXiv:1904.10153 (2019).
- [52] The BM Hamiltonian has an approximate particle-hole symmetry at small angles.
- [53] K. Hejazi, C. Liu, H. Shapourian, X. Chen, and L. Balents, Physical Review B **99**, 035111 (2019).
- [54] We thank Mike Zaletel for discussions on this point.

## SUPPLEMENTAL MATERIAL: Nematic insulating and semimetallic states in twisted bilayer graphene at charge neutrality

### SINGLE-PARTICLE PHYSICS: BISTRITZER-MACDONALD MODEL

Our starting point is the Bistritzer-MacDonald (BM) model of the TBG band structure [32], which we now briefly review. We begin with two layers of perfectly aligned (AA stacking) graphene sheets extended along the  $xy$  plane, and we choose the frame orientation such that the  $y$ -axis is parallel to some of the honeycomb lattice bonds. Now we choose an arbitrary atomic site and twist the top and bottom layers around that site by the counterclockwise angles  $\theta/2$  and  $-\theta/2$  (say  $\theta > 0$ ), respectively. When  $\theta$  is very small, the lattice form a Moiré pattern with very large translation vectors; correspondingly, the Moiré Brillouin zone (MBZ) is very small compared to the monolayer graphene Brillouin zone (BZ), as illustrated in Fig. S1. In this case, coupling between the two valleys can be neglected. If we focus on one of the two valleys, say  $K$ , then the effective Hamiltonian is given by:

$$\mathcal{H}_+ = \sum_l \sum_{\mathbf{k}} f_l^\dagger(\mathbf{k}) h_{\mathbf{k}}(l\theta/2) f_l(\mathbf{k}) + \left( \sum_{\mathbf{k}} \sum_{i=1}^3 f_i^\dagger(\mathbf{k} + \mathbf{q}_i) T_i f_b(\mathbf{k}) + h.c. \right). \quad (\text{S1})$$

Here,  $l = t/b \simeq \pm 1$  is the layer index, and  $f_l(\mathbf{k})$  is the  $K$ -valley electron originated from layer  $l$ . The sublattice index  $\sigma$  is suppressed, thus each  $f_l(\mathbf{k})$  operator is in fact a two-column vector.  $h_{\mathbf{k}}(\theta)$  is the monolayer graphene  $K$ -valley Hamiltonian with twist angle  $\theta$ :

$$h_{\mathbf{k}}(\theta) = \hbar v_F \begin{pmatrix} 0 & (k_x - ik_y)e^{i\theta} \\ (k_x + ik_y)e^{-i\theta} & 0 \end{pmatrix}, \quad (\text{S2})$$

where  $v_F = 9.1 \times 10^5$  m/s is the Fermi velocity. Let  $K_l$  be the  $K$ -vector of layer  $l$ , then  $\mathbf{q}_1$  is defined as  $K_b - K_t$ .  $\mathbf{q}_2 = O_3 \mathbf{q}_1$  is the counterclockwise  $120^\circ$  rotation of  $\mathbf{q}_1$ , and  $\mathbf{q}_3 = O_3 \mathbf{q}_2$ . Finally, the three matrices  $T_i$  are given by

$$T_1 = (1 + \beta) \begin{pmatrix} w_0 & w_1 \\ w_1 & w_0 \end{pmatrix}, \quad T_2 = \begin{pmatrix} w_0 & w_1 e^{-2\pi i/3} \\ w_1 e^{2\pi i/3} & w_0 \end{pmatrix}, \quad T_3 = \begin{pmatrix} w_0 & w_1 e^{2\pi i/3} \\ w_1 e^{-2\pi i/3} & w_0 \end{pmatrix}, \quad (\text{S3})$$

where we introduced an explicit  $C_3$ -breaking parameter  $\beta$ . We take  $w_1 = 110$  meV and  $w_0 = 82.5$  meV. The difference between  $w_0$  and  $w_1$  reflects the effect of lattice relaxation.

One intuitive way of thinking about this effective Hamiltonian is to imagine a honeycomb lattice of Dirac points in the momentum space, as shown in Fig. S2b, where the two sublattices correspond to the two layers. A Dirac point at momentum  $\mathbf{q}$  contributes a diagonal block  $h_{\mathbf{k}-\mathbf{q}}(\pm\theta/2)$  to the Hamiltonian for the MBZ momentum  $\mathbf{k}$ , where the sign is determined by the sublattice that  $\mathbf{q}$  belongs to. The off-diagonal blocks  $T_i$  are nothing but the nearest-neighbor couplings of these Dirac points.

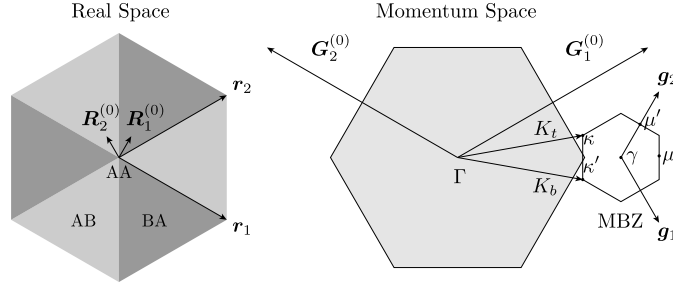


FIG. S1. Bravais lattice vectors, reciprocal lattice vectors and Brillouin zones for both monolayer and Moiré lattices of twisted bilayer graphene. In the real space (left) panel, we also show the underlying Moiré pattern structure.

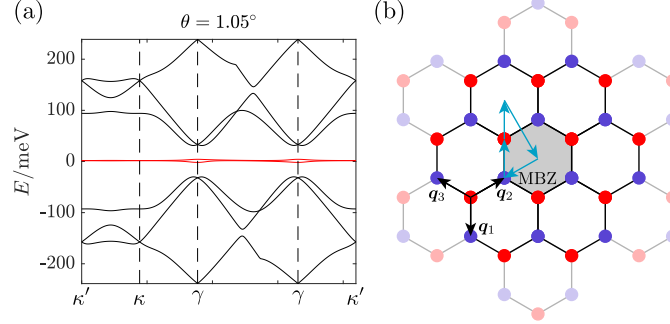


FIG. S2. (a) Band structure of magic-angle TBG obtained from the BM model. The sampling path is shown by the cyan arrows in the right panel. (b) Dirac point lattice at the MBZ.

When the twist angle is near the magic angle  $\theta = 1.05^\circ$ , two isolated flat bands per spin and valley appear near the charge neutrality (CN) Fermi energy, shown in Fig. S2a. These two bands are the focus of the current work.

The single particle Hamiltonian within each valley  $\mathcal{H}_\pm$  is invariant under the following symmetries

$$C_3 f_{\mathbf{k}} C_3^{-1} = e^{-\frac{2\pi}{3} i \tau_z \sigma_z} f_{C_3 \mathbf{k}}, \quad (C_2 \mathcal{T}) f_{\mathbf{k}} (C_2 \mathcal{T})^{-1} = \sigma_x f_{\mathbf{k}}, \quad \mathcal{M}_y f_{\mathbf{k}} \mathcal{M}_y^{-1} = \sigma_x \mu_x f_{M_y \mathbf{k}}, \quad (\text{S4})$$

In addition, the two valleys are related by time-reversal symmetry given by

$$\mathcal{T} f_{\mathbf{k}} \mathcal{T}^{-1} = \tau_x f_{-\mathbf{k}}. \quad (\text{S5})$$

Here,  $\sigma$ ,  $\tau$  and  $\mu$  denote the Pauli matrices in sublattice, valley and layer spaces, respectively.

### PROJECTING THE INTERACTION ONTO THE FLAT BANDS

In the following, we derive the form of the interaction when projecting onto the two flat bands. Since these two bands have a Wannier obstruction, we can only write such projected interaction in  $k$ -space. Let  $c_\alpha^\dagger(\mathbf{k})$  be the creation operator for the energy eigenstate in the band structure with internal flavor  $\mu$  and band index  $n$ , where  $\mu = (\tau, s)$  is a collective index including both valley  $\tau = \pm$  and spin  $s = \uparrow / \downarrow$ , and  $n = 1, 2$  represents the lower and upper bands, respectively. Also let  $f_{\mu, I}^\dagger(\mathbf{q})$  be the “elementary” continuous fermion with monolayer momentum  $\mathbf{q}$ , flavor  $\mu = (\tau, s)$  and  $I = (l, \sigma)$  representing layer and sublattice, then  $c^\dagger$  and  $f^\dagger$  are related to each other by the  $k$ -space wave functions as follows:

$$c_{\mu, n}^\dagger(\mathbf{k}) = \sum_{\mathbf{G}, I} u_{\tau, n; \mathbf{G}, I}(\mathbf{k}) f_{\mu, I}^\dagger(\mathbf{k} + \mathbf{G}), \quad (\text{S6})$$

where  $\mathbf{G}$  is a Moiré reciprocal lattice vector. In the above expression, we are already using the fact that the wave functions are spin-independent. Once we choose a gauge of  $u_{\tau, n; \mathbf{G}, I}(\mathbf{k})$  for all  $\mathbf{k}$  in some MBZ,  $c^\dagger(\mathbf{k})$  are defined in terms of the  $f^\dagger(\mathbf{q})$  for those  $\mathbf{k}$ , and whenever necessary, we define  $c^\dagger(\mathbf{k} + \mathbf{G}) = c^\dagger(\mathbf{k})$  for any reciprocal lattice vector  $\mathbf{G}$ , which is equivalent to defining  $u_{\tau, n; \mathbf{G}, I}(\mathbf{k} + \mathbf{G}_0) = u_{\tau, n; \mathbf{G} + \mathbf{G}_0, I}(\mathbf{k})$ . Note that the momentum argument for  $f^\dagger$  is unconstrained since we are



using the continuum theory for monolayers of graphene. We choose the normalization  $\{f_{\mu,I}(\mathbf{q}), f_{\mu',I'}^\dagger(\mathbf{q}')\} = \delta_{\mu\mu'}\delta_{II'}\delta_{\mathbf{q}\mathbf{q}'}$  (suppose the system size is finite), and  $\langle u_{\tau,n}(\mathbf{k}) | u_{\tau',n'}(\mathbf{k}') \rangle := \sum_{\mathbf{G},I} u_{\tau,n;\mathbf{G},I}^*(\mathbf{k}) u_{\tau',n';\mathbf{G},I}(\mathbf{k}') = \delta_{\tau\tau'}\delta_{nn'}$ , which imply  $\{c_{\mu,n}(\mathbf{k}), c_{\mu',n'}^\dagger(\mathbf{k}')\} = \delta_{\mu\mu'}\delta_{nn'}\delta_{\mathbf{k}\mathbf{k}'}$  when  $\mathbf{k}, \mathbf{k}'$  are confined in the MBZ. For the purpose of projecting the interaction into these two bands, it is convenient to introduce the form factor notation:

$$\lambda_{mn,\tau;\mathbf{G}}(\mathbf{k}_1, \mathbf{k}_2) := \langle u_{\tau,m}(\mathbf{k}_1) | u_{\tau,n}(\mathbf{k}_2 + \mathbf{G}) \rangle. \quad (\text{S7})$$

The form factors satisfy

$$\lambda_{mn,\tau;\mathbf{G}}(\mathbf{k}_1, \mathbf{k}_2) = \lambda_{nm,\tau;-\mathbf{G}}(\mathbf{k}_2, \mathbf{k}_1)^* \quad (\text{S8})$$

just from the definition, and also has the property

$$\lambda_{mn,\tau;\mathbf{G}}(\mathbf{k}_1, \mathbf{k}_2) = \lambda_{nm,-\tau;\mathbf{G}}(-\mathbf{k}_2, -\mathbf{k}_1) \quad (\text{S9})$$

due to the time-reversal symmetry.

The interaction Hamiltonian is given by

$$\mathcal{H}_{\text{int}} = \frac{1}{2A} \sum_{\sigma,\sigma',\tau,\tau'} \sum_{\mathbf{q}} V(\mathbf{q}) : \rho_{\sigma,\tau,\mathbf{q}} \rho_{\sigma',\tau',-\mathbf{q}} :, \quad (\text{S10})$$

where  $A$  is the total area of the system and  $V(\mathbf{q})$  is the momentum space interaction potential, related to the real-space one by  $V(\mathbf{q}) := \int d^2\mathbf{r} V(\mathbf{r}) e^{-i\mathbf{q}\cdot\mathbf{r}}$ . Depending on the number of gates,  $V(\mathbf{q})$  takes the following form in the SI units:

$$V(\mathbf{q}) = \frac{e^2}{2\epsilon\epsilon_0 q} \begin{cases} (1 - e^{-2qd_s}), & (\text{single-gate}) \\ \tanh(qd_s), & (\text{dual-gate}) \end{cases} \quad (\text{S11})$$

where the screening length  $d_s$  is nothing but the distance from the graphene plane to the gate(s). Projecting onto the two narrow bands, this Hamiltonian has the form

$$\begin{aligned} \mathcal{H}_{\text{int}} = \frac{1}{2A} \sum_{\sigma,\sigma',\tau,\tau'} \sum_{\mathbf{G},n_1,n_2,n_3,n_4} \sum_{\mathbf{k}_1,\mathbf{k}_2,\mathbf{k} \in \text{BZ}} \lambda_{n_1,n_2;\tau}(\mathbf{k}_1, \mathbf{k}_1 + \mathbf{k} + \mathbf{G}) V(\mathbf{G} + \mathbf{k}) \lambda_{n_4,n_3;\tau'}^*(\mathbf{k}_2, \mathbf{k}_2 + \mathbf{k} + \mathbf{G}) \\ \times c_{n_1,\sigma,\tau}^\dagger(\mathbf{k}_1) c_{n_3,\sigma',\tau'}^\dagger(\mathbf{k}_2 + \mathbf{k}) c_{n_4,\sigma',\tau'}(\mathbf{k}_2) c_{n_2,\sigma,\tau}(\mathbf{k}_1 + \mathbf{k}). \end{aligned} \quad (\text{S12})$$

### HARTREE-FOCK ANALYSIS IN THE CHIRAL LIMIT

The chiral limit of the BM model is obtained by switching off the  $w_0$  term in (S3) [48]. In this limit, the bands become exactly flat at the magic angle and the eigenstates of the Hamiltonian have a simple form similar to the Landau levels on a torus. In the following, we will assume that we are slightly off the magic angle so that we can still define the upper/lower bands (apart from the K and K' points) while at the same time having a very small bandwidth which can be neglected compared to the interaction term. In the chiral limit, the single particle Hamiltonian anticommutes with the chiral (sublattice) symmetry operator given by  $\Gamma = \sigma_z$ . In addition, it is invariant under the particle-hole symmetry  $\mathcal{P} f_{\mathbf{k}} \mathcal{P}^{-1} = i\sigma_x \mu_y f_{-\mathbf{k}}^\dagger$ .

Since chiral symmetry anticommutes with the Hamiltonian, it exchanges positive and negative energies, thus

$$\Gamma u_{1,\mathbf{k}} = e^{i\theta_{\mathbf{k}}} u_{2,\mathbf{k}}, \quad \Gamma u_{2,\mathbf{k}} = e^{-i\theta_{\mathbf{k}}} u_{1,\mathbf{k}} \quad (\text{S13})$$

The phase  $\theta_{\mathbf{k}}$  can be removed by a gauge transformation of the form  $e^{\frac{i}{2}\theta_{\mathbf{k}}\gamma_z}$ , where  $\gamma_{x,y,z}$  are the Pauli matrices in the band space, leading to  $\Gamma = \gamma_x$ . This leads to

$$\lambda_{11;\tau,\mathbf{G}}(\mathbf{k}, \mathbf{k}') = \lambda_{22;\tau,\mathbf{G}}(\mathbf{k}, \mathbf{k}') = \lambda_{\tau,\mathbf{G}}(\mathbf{k}, \mathbf{k}'), \quad \lambda_{12;\tau,\mathbf{G}}(\mathbf{k}, \mathbf{k}') = \lambda_{21;\tau,\mathbf{G}}(\mathbf{k}, \mathbf{k}') = \tilde{\lambda}_{\tau,\mathbf{G}}(\mathbf{k}, \mathbf{k}') \quad (\text{S14})$$

Similarly, the action of  $C_2\mathcal{T}$  is given by

$$C_2\mathcal{T} u_{1,\mathbf{k}} = e^{i\phi_{1,\mathbf{k}}} u_{1,\mathbf{k}}^*, \quad C_2\mathcal{T} u_{2,\mathbf{k}} = e^{i\phi_{2,\mathbf{k}}} u_{2,\mathbf{k}}^* \quad (\text{S15})$$

since  $C_2\mathcal{T}$  anticommutes with  $\Gamma$  in the original basis, it also has to anticommute with it in the band basis, which implies that

$\phi_{2,\mathbf{k}} = \phi_{1,\mathbf{k}} + \pi$ . We can remove the phase  $\phi_{\mathbf{k}}$  by a gauge transformation with the form  $e^{\frac{i}{2}\phi_{\mathbf{k}}}$  leading to  $C_2\mathcal{T} = \gamma_z\mathcal{K}$  with  $\mathcal{K}$  denoting complex conjugation. This leads to

$$\lambda_{\tau,G}(\mathbf{k}, \mathbf{k}') = \lambda_{\tau,G}^*(\mathbf{k}, \mathbf{k}'), \quad \tilde{\lambda}_{\tau,G}(\mathbf{k}, \mathbf{k}') = -\tilde{\lambda}_{\tau,G}^*(\mathbf{k}, \mathbf{k}') \quad (\text{S16})$$

Finally, we can use  $\mathcal{PT}$  symmetry to restrict the form factors further by noting that it acts similarly to  $\Gamma$  exchanging positive and negative energy eigenstates in opposite valleys

$$\mathcal{PT}u_{1,\tau,\mathbf{k}} = e^{i\eta_{\tau,\mathbf{k}}}u_{2,-\tau,\mathbf{k}}, \quad \mathcal{PT}u_{2,\tau,\mathbf{k}} = e^{-i\eta_{-\tau,\mathbf{k}}}u_{1,-\tau,\mathbf{k}} \quad (\text{S17})$$

The requirement of anticommutation with  $\Gamma$  and  $\tau_z$  and commutation with  $C_2\mathcal{T}$  fixes the phases  $\eta_{\tau,\mathbf{k}}$  such that  $\mathcal{PT} = \tau_x\gamma_y$  which implies that

$$\lambda_{\tau,G}(\mathbf{k}, \mathbf{k}') = \lambda_{-\tau,G}(\mathbf{k}, \mathbf{k}'), \quad \tilde{\lambda}_{\tau,G}(\mathbf{k}, \mathbf{k}') = -\tilde{\lambda}_{-\tau,G}(\mathbf{k}, \mathbf{k}') \quad (\text{S18})$$

which can be used to define a single intraband and interband form factors which are valley independent via

$$\lambda_{\tau,G}(\mathbf{k}, \mathbf{k}') = \lambda_G(\mathbf{k}, \mathbf{k}'), \quad \tilde{\lambda}_{\tau,G}(\mathbf{k}, \mathbf{k}') = \tau\tilde{\lambda}_G(\mathbf{k}, \mathbf{k}'), \quad \tau = \pm \quad (\text{S19})$$

We now investigate the Hartree-Fock solutions by looking for the minima of the Hartree-Fock energy. The Hartree-Fock energy is defined in terms of the order parameter

$$P_{\alpha\beta}(\mathbf{k}) = \langle c_{\alpha}^{\dagger}(\mathbf{k})c_{\beta}(\mathbf{k}) \rangle \quad (\text{S20})$$

where  $\alpha, \beta$  range over spin, valley and band indices. For an insulator or a semimetal, the number of filled states is  $\mathbf{k}$  independent and equal 4. This means that the order parameter  $P_{\mathbf{k}}$  is a projector satisfying

$$P(\mathbf{k})^2 = P(\mathbf{k}) = P^{\dagger}(\mathbf{k}), \quad \text{tr } P(\mathbf{k}) = 4 \quad (\text{S21})$$

The Hartree-Fock energy can then be written as (using properties of the chiral limit)

$$E_{\text{HF}} = E_H + E_F, \quad (\text{S22})$$

$$E_H = \frac{1}{2A} \sum_{\mathbf{G}, \mathbf{k}, \mathbf{k}'} V_{\mathbf{G}} \text{tr } P(\mathbf{k}) \Lambda_{\mathbf{G}}^{\dagger}(\mathbf{k}, \mathbf{k}') \text{tr } P(\mathbf{k}') \Lambda_{\mathbf{G}}(\mathbf{k}', \mathbf{k}'), \quad (\text{S23})$$

$$E_F = -\frac{1}{2A} \sum_{\mathbf{G}, \mathbf{k}, \mathbf{k}'} V_{\mathbf{G}+\mathbf{k}'-\mathbf{k}} \text{tr } P(\mathbf{k}) \Lambda_{\mathbf{G}}^{\dagger}(\mathbf{k}, \mathbf{k}') P(\mathbf{k}') \Lambda_{\mathbf{G}}(\mathbf{k}, \mathbf{k}') \quad (\text{S24})$$

where we defined the form factor matrix  $\Lambda_{\mathbf{G}}(\mathbf{k}, \mathbf{k}')$  in terms of the combined index  $\alpha = (s, \tau, n)$  for spin, valley, and band as

$$[\Lambda_{\mathbf{G}}(\mathbf{k}, \mathbf{k}')]_{\alpha, \alpha'} = \delta_{s,s'} \delta_{\tau,\tau'} \lambda_{nn';\tau,G}(\mathbf{k}, \mathbf{k}') = \delta_{\sigma,\sigma'} \delta_{\tau,\tau'} [\lambda_{\mathbf{G}}(\mathbf{k}, \mathbf{k}') \gamma_0 + \tau \tilde{\lambda}_{\mathbf{G}}(\mathbf{k}, \mathbf{k}') \gamma_x]_{n,n'} \quad (\text{S25})$$

which satisfies  $\Lambda_{\mathbf{G}}(\mathbf{k}, \mathbf{k}')^T = \Lambda_{\mathbf{G}}(\mathbf{k}, \mathbf{k}')$ . The form factors decay in the separation  $\mathbf{G} + \mathbf{k}' - \mathbf{k}$  with a characteristic scale  $\kappa$  which is typically smaller than the size of the Brillouin zone. This means that the sums in the Hartree and Fock terms are dominated by the  $\mathbf{G} = 0$  term. For the Hartree term, this equals  $4V(0)N$  and is independent of the order parameter  $P(\mathbf{k})$ . Thus, the Hartree term has little effect on the competition between different phases and will be neglected in the following.

We now consider possible types of symmetry-broken orders at charge neutrality. The order parameter  $P(\mathbf{k})$  can generally be written as

$$P(\mathbf{k}) = \frac{1}{2}[1 + Q(\mathbf{k})], \quad \text{tr } Q(\mathbf{k}) = 0 \quad (\text{S26})$$

Since the Fock term is the largest contribution to the mean-field energy, let us now neglect the Hartree term as well as the single-particle term  $h_0$ . We note that  $\langle A, B \rangle = \text{tr } AB$  defines a positive definite inner product on the space of hermitian matrices. Using Cauchy-Schwarz inequality, we get

$$E_F \geq -\frac{1}{2A} \sum_{\mathbf{k}, \mathbf{k}', \mathbf{G}} V_{\mathbf{G}+\mathbf{k}'-\mathbf{k}} \sqrt{\text{tr } P(\mathbf{k}) \text{tr} [\Lambda_{\mathbf{G}}^{\dagger}(\mathbf{k}, \mathbf{k}') P(\mathbf{k}') \Lambda_{\mathbf{G}}(\mathbf{k}, \mathbf{k}')]^2} \quad (\text{S27})$$

We now note that

$$\Lambda_G(\mathbf{k}, \mathbf{k}') \Lambda_G^\dagger(\mathbf{k}, \mathbf{k}') = \Lambda_G^\dagger(\mathbf{k}, \mathbf{k}') \Lambda_G(\mathbf{k}, \mathbf{k}') = \gamma_0 \tau_0 (|\lambda_G(\mathbf{k}, \mathbf{k}')|^2 + |\tilde{\lambda}_G(\mathbf{k}, \mathbf{k}')|^2) \quad (\text{S28})$$

This implies that we can write  $\Lambda_G(\mathbf{k}, \mathbf{k}')$  as

$$\Lambda_G(\mathbf{k}, \mathbf{k}') = R_G(\mathbf{k}, \mathbf{k}') U_G(\mathbf{k}, \mathbf{k}'), \quad U_G(\mathbf{k}, \mathbf{k}') = e^{i\Phi_G(\mathbf{k}, \mathbf{k}')\gamma_x\tau_z}, \quad R_G(\mathbf{k}, \mathbf{k}') = (|\lambda_G(\mathbf{k}, \mathbf{k}')|^2 + |\tilde{\lambda}_G(\mathbf{k}, \mathbf{k}')|^2) \quad (\text{S29})$$

Substituting in (S27) yields

$$E_F \geq -\frac{2}{A} \sum_{\mathbf{k}, \mathbf{k}', G} V_{G+\mathbf{k}'-\mathbf{k}} R_G(\mathbf{k}, \mathbf{k}') \quad (\text{S30})$$

This inequality is satisfied if and only if  $P(\mathbf{k}')$  is parallel to  $\Lambda_G(\mathbf{k}, \mathbf{k}') P(\mathbf{k}) \Lambda_G^\dagger(\mathbf{k}, \mathbf{k}')$  for every  $\mathbf{k}, \mathbf{k}'$  and  $G$ . This means

$$P(\mathbf{k}') = U_G(\mathbf{k}, \mathbf{k}') P(\mathbf{k}) U_G^\dagger(\mathbf{k}, \mathbf{k}') \Rightarrow Q(\mathbf{k}') = U_G(\mathbf{k}, \mathbf{k}') Q(\mathbf{k}) U_G^\dagger(\mathbf{k}, \mathbf{k}') \quad (\text{S31})$$

#### Flavor-polarized states

A  $\mathbf{k}$ -independent flavor (spin, valley) polarized state obviously satisfies this constraint since  $U_G(\mathbf{k}, \mathbf{k}')$  is diagonal in flavor, thereby saturating the Fock bound. This state can either be spin-polarized  $Q = s_z$ , valley polarized  $Q = \tau_z$  or spin-valley locked  $Q = \tau_z s_z$ .

#### $C_2\mathcal{T}$ breaking

A  $C_2\mathcal{T}$  breaking solution to Eq. S31 is obtained by taking  $Q_{\mathbf{k}} = \gamma_x$  (recall that  $C_2\mathcal{T} = \gamma_z \mathcal{K}$ ). The resulting state saturates the Fock bound and is characterized by a Chern number  $\pm 1$  in the lower band. Its energy competition with the flavor-polarized states is settled by the effects of the single-particle term  $h_0$  and  $w_0$  which are neglected here. In our numerics, we found that these states are almost degenerate for the realistic model with their energy difference only sensitive to the strain parameter  $\beta$ . Depending on its structure in flavor space, the  $C_2\mathcal{T}$ -breaking insulator may correspond to one of four states: (i)  $Q = s_0 \tau_0 \gamma_x$  breaks  $C_2$  but not  $\mathcal{T}$  and corresponds to a valley Hall state, (ii)  $Q = s_0 \tau_z \gamma_x$  breaks  $\mathcal{T}$  but not  $C_2$  and corresponds to a quantum Hall state with Chern number  $\pm 4$ , (iii)  $Q = s_z \tau_0 \gamma_x$  corresponds to a valley-spin-Hall state where the Chern number is invariant under flipping spin and valley, and (iv)  $Q = s_z \tau_z \gamma_x$  corresponds to a spin-Hall state.

#### $C_3$ breaking

A  $\mathbf{k}$ -independent order parameter which does not break  $C_2\mathcal{T}$  cannot satisfy Eq. S31. However, there could still be solutions which are  $\mathbf{k}$ -dependent. A general  $C_2\mathcal{T}$ -invariant solution is given by

$$Q(\mathbf{k}) = \gamma_z \cos \alpha_{\mathbf{k}} + \gamma_y \sin \alpha_{\mathbf{k}} = \gamma_z e^{i\alpha_{\mathbf{k}}\gamma_x} \quad (\text{S32})$$

Substituting in the Fock energy (S24) yields

$$E_F = -\frac{1}{A} \sum_{G, \mathbf{k}, \mathbf{k}'} V_{G+\mathbf{k}'-\mathbf{k}} R_G(\mathbf{k}, \mathbf{k}') \{1 + \cos[\alpha_{\mathbf{k}} - \alpha_{\mathbf{k}'+G} + 2\Phi_G(\mathbf{k}, \mathbf{k}')]\} \quad (\text{S33})$$

where we used periodicity of  $\alpha_{\mathbf{k}}$  (which follows from the periodicity of  $P(\mathbf{k})$ ). To simplify further, we first note that in the chosen gauge, the Berry connection defined as

$$[\mathcal{A}(\mathbf{k})]_{\alpha, \beta} = -i \langle u_{\alpha, \mathbf{k}} | \nabla_{\mathbf{k}} | u_{\beta, \mathbf{k}} \rangle \quad (\text{S34})$$

has the simple form  $\mathcal{A}(\mathbf{k}) = A_{\mathbf{k}} \gamma_x \tau_z$ , with  $A_{\mathbf{k}}$  satisfying  $\frac{1}{2\pi} \int_{\text{BZ}} \nabla_{\mathbf{k}} \times A_{\mathbf{k}} = 1$ . Furthermore, we assume  $R_G(\mathbf{k}, \mathbf{k}')$  decays with the relative momentum  $\mathbf{k}' + \mathbf{G} - \mathbf{k}$ , so that we can expand  $\Phi_G(\mathbf{k}, \mathbf{k}')$  and  $\alpha_{\mathbf{k}'+G}$ . Noting that  $\Phi_G(\mathbf{k}, \mathbf{k}') = (\mathbf{k}' + \mathbf{G} - \mathbf{k}) \cdot \mathbf{A}_{\mathbf{k}}$

to leading order and assuming the magnitude of the form factor  $R_G(\mathbf{k}, \mathbf{k}')$  depends only on  $(\mathbf{k}' + \mathbf{G} - \mathbf{k})$ , we get the expression

$$E_F = -\frac{2}{A} \sum_{\mathbf{G}, \mathbf{k}, \mathbf{k}'} V_{\mathbf{G}+\mathbf{k}'-\mathbf{k}} R_G(\mathbf{k}, \mathbf{k}') + \frac{\kappa}{2} \sum_{\mathbf{k}} (\nabla_{\mathbf{k}} \alpha_{\mathbf{k}} - 2\mathbf{A}_{\mathbf{k}})^2, \quad \kappa = \frac{1}{A} \sum_{\mathbf{G}, \mathbf{k}'} V_{\mathbf{G}+\mathbf{k}'-\mathbf{k}} (\mathbf{G} + \mathbf{k}' - \mathbf{k})^2 R_G(\mathbf{k}, \mathbf{k}') \quad (\text{S35})$$

It is impossible to make the second term vanish for the following reason. Since the band basis is singular at the Moiré K and K' points  $\mathbf{A}_{\mathbf{k}}$  is also singular at these points and can be expressed as  $\mathbf{A}_{\mathbf{k}} = \frac{1}{2} \nabla_{\mathbf{k}} \phi_{\mathbf{k}}$  where  $\phi_{\mathbf{k}} = \arg(k_x + ik_y)$ . Thus, to minimize the second term we need to choose  $\alpha_{\mathbf{k}} = \phi_{\mathbf{k}}$  in the vicinity of Moiré K and K' points. However, since the Dirac points at K and K' is the same, this leads to an overall winding of  $4\pi$  of  $\alpha_{\mathbf{k}}$  over the Brillouin zone which is inconsistent with periodicity. To resolve this issue, there has to be at least two other points in the Brillouin zone where the winding of the phase  $\alpha_{\mathbf{k}}$  is  $-2\pi$  so that the overall phase winding is zero. These points represent vortices in the order parameter and will cost energy implying that the Fock energy will be larger than the Fock bound. The location of these points is determined by the requirement that the Fock energy is minimized and depends sensitively on the  $\mathbf{k}$ -dependence of  $\mathbf{A}_{\mathbf{k}}$ . Numerically, we see that this happens when both vortices are placed very close to the  $\Gamma$  point. The Fock energy of the resulting state is strictly larger than the Fock bound, but it may gain energetically from other terms  $h_0$  and  $w_0$  neglected here.

The order parameter obtained numerically from the self-consistent Hartree-Fock analysis is shown in Fig. S3. We notice that  $Q_{+, \mathbf{k}}$  is discontinuous at K, K' and at two points very close to  $\Gamma$ . The discontinuity at K and K' is an artefact of the band basis which is discontinuous at these two points and it cancels against the discontinuity in the band basis leading to a continuous projector when expressed in the original basis. On the other hand, the discontinuities near  $\Gamma$  corresponds an actual singularity for the projection operator onto the filled bands at this point indicating that the corresponding phase is a semimetal. This can be verified by comparing the numerically obtained order parameter and with a simple order parameter  $\alpha_{\mathbf{k}} = 2\phi_{\mathbf{k}} - \phi_{\mathbf{k}-K} - \phi_{\mathbf{k}-K'}$  corresponding to placing both vortices at  $\Gamma$  as shown in Fig. S3.

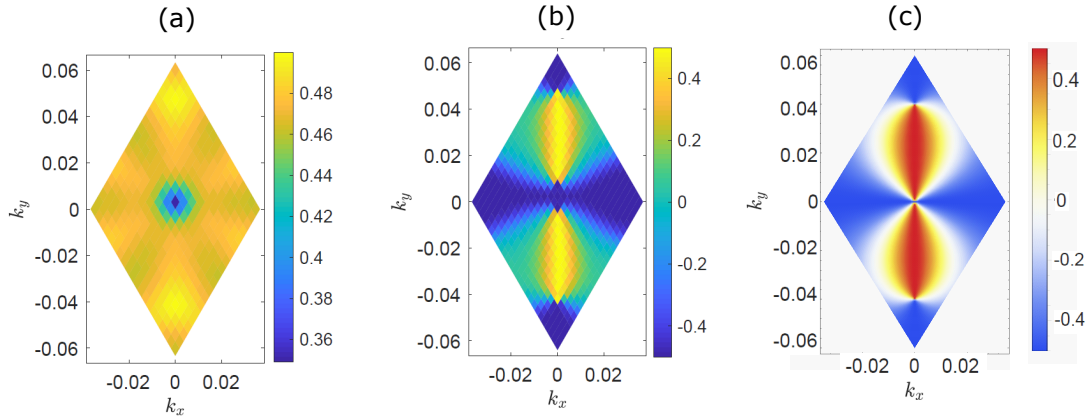


FIG. S3. (a)  $\gamma_x$  component of the  $C_2\mathcal{T}$  order parameter,  $\frac{1}{2} \text{tr } P(\mathbf{k})\gamma_x$ , obtained from solving the self-consistent equation numerically (with  $w_0 \neq 0$ ). We see that it is relatively uniform over the BZ consistent with our ansatz. (b)  $\gamma_z$  component for the  $C_3$ -breaking order  $\frac{1}{2} \text{tr } P(\mathbf{k})\gamma_z$  obtained from solving the self-consistent equation numerically (with  $w_0 \neq 0$ ). (c)  $\gamma_z$  component of the order parameter for a simple ansatz for the order parameter in the chiral limit given by  $-\frac{1}{2} \cos \alpha_{\mathbf{k}}$ ,  $\alpha_{\mathbf{k}} = 2\phi_{\mathbf{k}} - \phi_{\mathbf{k}-K} - \phi_{\mathbf{k}-K'}$

### Intervalley coherent states

Let us now briefly discuss states which break U(1) valley symmetry. These states were argued to be energetically unfavorable in the context of twisted bilayer graphene with an aligned hBN substrate [36] and other Moiré materials which lack  $C_2$  symmetry [17, 22]. Here, we will show that a similar argument fails [54] in  $C_2$ -symmetric twisted bilayer graphene due to the extra particle-hole symmetry  $\mathcal{P}$  which is exact in the chiral limit. A more detailed discussion of such phases is provided in Ref. [46]. To clarify the importance of  $\mathcal{P}$ , we will assume that the symmetry is not present in which case, the form factors in the two opposite valleys at the same momentum  $\mathbf{k}$  are not related, i.e.  $R_{+, \mathbf{G}}(\mathbf{k}, \mathbf{k}') \neq R_{-, \mathbf{G}}(\mathbf{k}, \mathbf{k}')$ . Furthermore, we will assume unbroken time-reversal symmetry. The case of time-reversal symmetry breaking can be addressed similarly. The projector for an IVC state can be split into a diagonal and off-diagonal component in valley space

$$P(\mathbf{k}) = P_d(\mathbf{k}) + P_o(\mathbf{k}), \quad P_d(\mathbf{k})^2 + P_o(\mathbf{k})^2 = P_d(\mathbf{k}), \quad (\text{S36})$$

In terms of valley resolved blocks of  $P(\mathbf{k})$ , i.e.

$$P = \begin{pmatrix} P_+ & P_{12} \\ P_{21} & P_- \end{pmatrix}, \quad (\text{S37})$$

the second condition can be written as

$$P_+^2 + P_{12}P_{21} = P_+, \quad P_-^2 + P_{21}P_{12} = P_-. \quad (\text{S38})$$

Since the form factors are diagonal in valley space, the Fock energy can be written as a sum of a term with only diagonal part and one with only off-diagonal parts as

$$\begin{aligned} E_F &= -\frac{1}{2A} \sum_{\mathbf{G}, \mathbf{k}, \mathbf{k}'} V_{\mathbf{G}+\mathbf{k}'-\mathbf{k}} \text{tr}[P_d(\mathbf{k})\Lambda_{\mathbf{G}}^\dagger(\mathbf{k}, \mathbf{k}')P_d(\mathbf{k}')\Lambda_{\mathbf{G}}(\mathbf{k}, \mathbf{k}') + P_o(\mathbf{k})\Lambda_{\mathbf{G}}^\dagger(\mathbf{k}, \mathbf{k}')P_o(\mathbf{k}')\Lambda_{\mathbf{G}}(\mathbf{k}, \mathbf{k}')] \\ &\geq -\frac{1}{2A} \sum_{\mathbf{G}, \mathbf{k}, \mathbf{k}'} V_{\mathbf{G}+\mathbf{k}'-\mathbf{k}} [R_{+, \mathbf{G}}(\mathbf{k}, \mathbf{k}')^2 \sqrt{\text{tr } P_+(\mathbf{k})^2 \text{tr } P_+(\mathbf{k}')^2} + R_{-, \mathbf{G}}(\mathbf{k}, \mathbf{k}')^2 \sqrt{\text{tr } P_-(\mathbf{k})^2 \text{tr } P_-(\mathbf{k}')^2} \\ &\quad + R_{+, \mathbf{G}}(\mathbf{k}, \mathbf{k}')R_{-, \mathbf{G}}(\mathbf{k}, \mathbf{k}')\sqrt{\text{tr } P_o(\mathbf{k})^2 \text{tr } P_o(\mathbf{k}')^2}] \\ &\geq -\frac{1}{2A} \sum_{\mathbf{G}, \mathbf{k}, \mathbf{k}'} V_{\mathbf{G}+\mathbf{k}'-\mathbf{k}} [R_{+, \mathbf{G}}(\mathbf{k}, \mathbf{k}') \text{tr } P_+(\mathbf{k})^2 + R_{-, \mathbf{G}}(\mathbf{k}, \mathbf{k}') \text{tr } P_-(\mathbf{k})^2 + R_{+, \mathbf{G}}(\mathbf{k}, \mathbf{k}')R_{-, \mathbf{G}}(\mathbf{k}, \mathbf{k}') \text{tr } P_o(\mathbf{k})^2] \\ &= -\frac{1}{2A} \sum_{\mathbf{G}, \mathbf{k}, \mathbf{k}'} V_{\mathbf{G}+\mathbf{k}'-\mathbf{k}} [R_{+, \mathbf{G}}(\mathbf{k}, \mathbf{k}') \text{tr}(P_+(\mathbf{k}) - P_{12}(\mathbf{k})P_{21}(\mathbf{k})) + R_{-, \mathbf{G}}(\mathbf{k}, \mathbf{k}') \text{tr}(P_-(\mathbf{k}) - P_{21}(\mathbf{k})P_{12}(\mathbf{k})) \\ &\quad + 2R_{+, \mathbf{G}}(\mathbf{k}, \mathbf{k}')R_{-, \mathbf{G}}(\mathbf{k}, \mathbf{k}') \text{tr}(P_{12}(\mathbf{k})P_{21}(\mathbf{k}))] \\ &= -\frac{\nu}{2A} \sum_{\mathbf{G}, \mathbf{k}, \mathbf{k}'} V_{\mathbf{G}+\mathbf{k}'-\mathbf{k}} R_{+, \mathbf{G}}(\mathbf{k}, \mathbf{k}') + \frac{1}{4A} \sum_{\mathbf{G}, \mathbf{k}, \mathbf{k}'} V_{\mathbf{G}+\mathbf{k}'-\mathbf{k}} (R_{+, \mathbf{G}}(\mathbf{k}, \mathbf{k}') - R_{-, \mathbf{G}}(\mathbf{k}, \mathbf{k}'))^2 \text{tr } P_o(\mathbf{k})^2, \end{aligned} \quad (\text{S39})$$

where time reversal symmetry is used to obtain the last line. If the second term is non-zero, then we would conclude that the Fock energy for the IVC is larger than the energy bound for the valley polarized or unpolarized phases by an amount which is proportional to the valley off-diagonal part of the order parameter. This energy difference in (S39) is generally not expected to be small and receives contribution from  $\mathbf{G} = 0$ . However, the existence of extra hidden particle-hole symmetry  $\mathcal{P}$  in the model [46] implies  $R_{+, \mathbf{G}}(\mathbf{k}, \mathbf{k}') = R_{-, \mathbf{G}}(\mathbf{k}, \mathbf{k}')$ , forcing the second term to vanish which makes the bound (S39), while correct, inconclusive to rule out IVC states.

### EFFECT OF IN-PLANE MAGNETIC FIELD

To study the effect of the in-plane field, we choose the gauge  $\mathbf{A}_l = -(ld/2) \hat{z} \times \mathbf{B}$  for the two layers, with  $d = 3.42 \text{ \AA}$  being the interlayer distance. Such gauge choice preserves the two-dimensional translation symmetry since it is just a constant within each layer. Thus, to leading order, the change of a band structure due to the orbital effect can be written as

$$\delta\xi_{n, \tau}(\mathbf{k}; \mathbf{B}) = \mu_B \mathbf{g}_{n, \tau}(\mathbf{k}) \cdot \mathbf{B}, \quad (\text{S40})$$

where  $\mathbf{g}_{n, \tau}(\mathbf{k})$  is a  $\mathbf{k}$ -dependent orbital  $g$ -factor. Following Ref. [22], we compute  $\mathbf{g}_n(\mathbf{k})$  by taking the expectation value of the term proportional to  $\mathbf{B}$  in the minimally coupled BM model leading to

$$\mathbf{g}_{n, \tau}(\mathbf{k}) = g_0 \langle u_{n, \tau, \mathbf{k}} | \mu_z (-\sigma_y, \tau \sigma_x) | u_{n, \tau, \mathbf{k}} \rangle \quad (\text{S41})$$

with  $u_{n, \tau, \mathbf{k}}$  denoting the eigenstates of the BM Hamiltonian and  $\sigma$  and  $\mu$  denoting the Pauli matrices in the sublattice and layer spaces, respectively.  $g_0 := ev_F d / (2\mu_B) = 2.68$  is a dimensionless constant ( $v_F$  being the Fermi velocity of monolayer graphene) measuring the strength of the in-plane orbital effect which is comparable to the electron spin  $g$ -factor  $g_s \approx 2$ . We note that  $\mathbf{g}_{n, \tau}(\mathbf{k})$  vanishes at the  $\Gamma$  point as long as  $C_3$  symmetry is unbroken.

At CN, the insulating solutions are the SP, VP and  $C_2\mathcal{T}$ -breaking states. Without any strain, in all these cases, the maximum of the filled bands and the minimum of the empty bands occur at the  $\Gamma$  point where the orbital  $g$ -factor vanishes due to the  $C_3$  symmetry. Thus, for experimentally accessible magnetic fields ( $|\mathbf{B}| < 10 \text{ T}$ ), the orbital effect does not play a role. Therefore, the only effect of in-plane field comes from the spin Zeeman term, which linearly increases the gap of the SP states and decreases

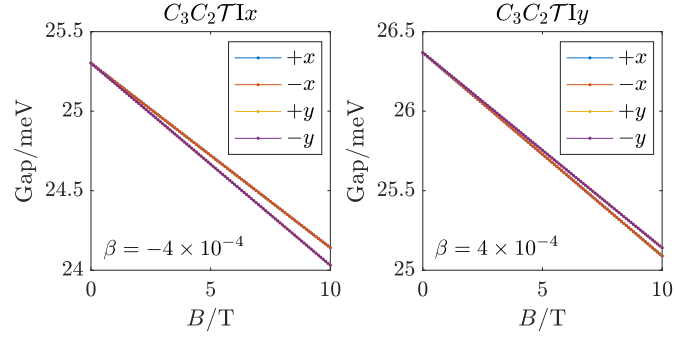


FIG. S4. Gaps of the  $C_3C_2\mathcal{T}lx$  (left) and  $C_3C_2\mathcal{T}ly$  (right) states as functions of in-plane magnetic fields applied in  $\pm x$  or  $\pm y$  directions. In both cases, the  $+x$  and  $+y$  curves overlap with the  $-x$  and  $-y$  curves, respectively.

the gaps of the VP and  $C_2\mathcal{T}$ -breaking states with a slope of roughly 0.1 meV/T. In the presence of strain, the  $C_3C_2\mathcal{T}lx, y$  states largely break the  $C_3$  symmetry, thus there can be a nonzero orbital effect. In Fig. S4, we plot the gaps of the  $C_3C_2\mathcal{T}lx, y$  states as functions of in-plane fields applied in the  $\pm x$  or  $\pm y$  directions. The spin Zeeman effect still dominates and reduces the gaps, but a small anisotropy is generated due to the orbital  $g$ -factor. For the VP/SP states, small  $C_3$  breaking has negligible effect on the  $g$  factor and the energy spectrum, leading to very small orbital effect.